PNAS RESEARCH ARTICLE | CELL BIOLOGY

FAO-fueled OXPHOS and NRF2-mediated stress resilience in MICs drive lymph node metastasis

Shan-Shan Li[a,b,1,2], Baifeng Zhang[c,1], Cuicui Huang[c], Yuying Fu[b], Yuying Zhao[a], Lanqi Gong[c], Yanan Tan[a,b], Huali Wang[a], Wenqi Chen[a], Jie Luo[c], Yu Zhang[d], Stephanie Ma[a,e], Li Fu[f], Chenli Liu[g], Jiandong Huang[e,g], Huai-Qiang Ju[a,d], Anne Wing-Mui Lee[a,c], and Xin-Yuan Guan[a,b,c,d,2]

Affiliations are included on p. 9.

Edited by Tak Mak, University of Toronto, Toronto, ON, Canada; received June 5, 2024; accepted February 25, 2025

Metastasis is an inefficient process requiring cancer cells to adapt metabolically for survival and colonization in new environments. The contributions of tumor metabolic reprogramming to lymph node (LN) metastasis and its underlying mechanisms remain elusive. Through single-cell RNA sequencing, we identified rare metastasis-initiating cells (MICs) with stem-like properties that drive early LN metastasis. Integrated transcriptome, lipidomic, metabolomic, and functional analyses demonstrated that MICs depend on oxidative phosphorylation (OXPHOS) fueled by fatty acid oxidation (FAO) in the lipid-rich LN microenvironment. Mechanistically, the NRF2-SLC7A11 axis promotes glutathione synthesis to mitigate oxidative stress, thereby enhancing stress resistance and metastatic potential of MICs. Inhibition of NRF2-SLC7A11 reduced LN metastasis and sensitized tumors to cisplatin. Clinically, elevated NRF2-SLC7A11 expression was observed in tumors, with high expression correlating with LN metastasis, chemoresistance, and poor prognosis in esophageal squamous cell carcinoma (ESCC). These findings highlight the pivotal roles of FAO-fueled OXPHOS and NRF2 in LN metastasis and suggest targeting these pathways as a promising therapeutic strategy for metastatic ESCC.

lymph node metastasis | metabolic reprogramming | oxidative phosphorylation | NRF2 | esophageal cancer

Significance

Lymph node (LN) metastasis is a critical step in cancer progression, yet the metabolic adaptations that enable tumor cells to survive and colonize this microenvironment remain unclear. This study identifies a rare subpopulation of metastasis-initiating cells (MICs) that drive early LN metastasis by relying on fatty acid oxidation (FAO)–fueled oxidative phosphorylation (OXPHOS) for energy production in the lipid-rich LN niche. NRF2-SLC7A11 signaling enhances MIC stress resilience by promoting glutathione synthesis and mitigating oxidative stress. Targeting FAO-OXPHOS metabolism and NRF2-mediated stress resistance represents a promising therapeutic strategy for improving treatment outcomes in metastatic esophageal cancer.

Metastasis is the principal cause of mortality in esophageal squamous cell carcinoma (ESCC), with lymph node (LN) metastasis being a pivotal early event that often dictates subsequent systemic spread and poor prognosis (1, 2). Most previous studies of tumor metastasis have focused on distant metastasis, leaving fundamental questions about how tumor cells survive in LNs largely unanswered.

Throughout the metastatic cascade, disseminating tumor cells face strong selective pressure, and only a small subset possesses the ability to establish manifest metastases (2–4). This inefficiency suggests the existence of a specialized population known as metastasis-initiating cells (MICs), which possess unique adaptive properties that enable metastatic colonization (5). Increasing evidence indicates that MICs within heterogeneous tumor populations exhibit distinct metabolic programs that facilitate their survival in new microenvironments (6).

Metabolic reprogramming is a hallmark of tumors, essential for their development and progression (7). Tumor cells dynamically adjust multiple metabolic pathways to meet energy and biosynthetic demands, adapting to the varying nutrient availability across metastatic niches (8, 9). Emerging evidence suggests that MICs exhibit a distinct metabolic program that enables them to endure the metabolic stress of dissemination (10, 11). In particular, MICs in breast cancer and oral squamous cell carcinoma have been shown preferentially utilize dietary lipids as a primary energy source, fueling fatty acid oxidation (FAO) and the oxidative tricarboxylic acid cycle to sustain their metastatic potential (12, 13). Additionally, upregulation of oxidative phosphorylation (OXPHOS) has been observed in micrometastases of various cancers, with pharmacological inhibition of mitochondrial respiration impairing metastatic seeding (14). Despite these insights, the metabolic dependencies of MICs in ESCC and their role in LN metastasis remain largely unexplored.

During metastasis, tumor cells encounter oxidative stress due to increased mitochondrial respiration and fluctuating nutrient availability (15). To survive these challenges, metastatic cells require adaptive mechanisms to maintain redox balance (8, 16, 17). Nuclear factor-erythroid 2-related factor 2 (NFE2L2, NRF2), a key transcriptional regulator of oxidative stress response, modulates redox homeostasis and lipid peroxidation defense (18). While NRF2 activation has been implicated in tumor progression and

Author contributions: S.-S.L., B.Z., and X.-Y.G. designed research; S.L., B.Z., C.H., Y.F., Y. Zhao, L.G., Y.T., W.C., J.L., Y. Zhang, and X.-Y.G. performed research; B.Z., S.M., L.F., C.L., J.H., H.-Q.J., and A.W.-M.L. contributed new reagents/analytic tools; S.-S.L., B.Z., C.H., Y.F., Y. Zhao, L.G., Y.T., H.W., W.C., J.L., and Y. Zhang analyzed data; and S.-S.L. and B.Z. wrote the paper.

The authors declare no competing interest.

This article is a PNAS Direct Submission.

[1]S.-S.L. and B.Z. contributed equally to this work.

[2]To whom correspondence may be addressed. Email: liss3@hku-szh.org or xyguan@hku.hk.

This article contains supporting information online at https://www.pnas.org/lookup/suppl/doi:10.1073/pnas.2411241122/-/DCSupplemental.

Published April 11, 2025.

chemoresistance, its role in metastatic adaptation remains incompletely understood (19–21). However, how redox regulation interacts with metabolic adaptation and stress resilience of MICs requires further investigation to determine its contribution to LN metastasis.

Single-cell RNA (scRNA-seq) sequencing has revolutionized our understanding of tumor heterogeneity by analyzing transcriptome diversity within tumors at high resolution (14). This technology is particularly effective in identifying the metabolic profiles of rare cell populations with high metastatic potential, such as MICs. Furthermore, scRNA-seq can trace the metabolic evolution of tumors over time, providing a temporal aspect to our comprehension of tumor metabolism. These insights are crucial for unraveling the metabolic adaptations underlying metastasis.

In this study, we employed scRNA-seq, lipidomic, and metabolic profiling to explore the properties of metastatic tumor cells in a human xenograft model of spontaneous LN metastasis (Fig. 1). Our findings identify MICs as a key subpopulation driving early LN metastasis, with a reliance on FAO-fueled OXPHOS. Additionally, NRF2-regulated glutathione (GSH) synthesis supports MIC survival and adaptation within the LN environment. These results highlight metabolic vulnerabilities and antioxidant pathways as promising therapeutic targets for combating LN metastasis in ESCC.

Results

Establishment of a Xenograft Model for Analyzing LN Metastasis in ESCC. To investigate the LN metastatic progression of ESCC, we established a xenograft spontaneous ankle-popliteal LN metastasis model in mice. In this model, GFP-labeled human ESCC KYSE-180 cells were injected into the hocks of nude mice, enabling real-time visualization of tumor growth and metastasis in vivo (*SI Appendix,* Fig. S1 *A* and *B*). Within 2 to 3 wk postinoculation, micrometastases (micromet) were observed in the popliteal LN, with most mice displaying sporadic, low-density metastases near the LN margin. At this stage, the proportion of metastatic tumor cells in the popliteal LN was below 0.1%, with approximately 50 to 100 disseminated tumor cells (*SI Appendix,* Fig. S1*C*). By 5 to 6 wk, macrometastases (macromet) had developed, occupying the popliteal LN in half of the mice (*SI Appendix,* Fig. S1*D*). This progression allowed us to assess the varying degrees of metastasis and to explore the early events of metastatic seeding and colonization at more advanced stages.

Single-Cell Transcriptomics Reveal Intratumor Heterogeneity and Molecular Signatures of LN Metastasis. To investigate the intratumor heterogeneity and molecular characteristics associated with LN metastasis, we conducted a comparative single-cell transcriptomics analysis on tumor cells harvested from various stages of metastatic LNs in mice. Tumor cells were collected from 20 primary tumors, 35 LNs with micromet, and 3 LNs with macromet, then pooled for single-cell RNA sequencing. After rigorous quality control and doublet removal processes, we analyzed a total of 18,577 cells, which included 7,334 from primary tumors, 2,037 from micromet, and 9,206 from macromet LNs.

Utilizing principal component analysis and the Uniform Manifold Approximation and Projection (UMAP) algorithm, we identified eighteen distinct subclusters showing differential gene expression patterns, highlighting the extensive heterogeneity within tumor cell populations (Fig. 2*A*). Gene Ontology analysis of highly expressed gene markers allowed us to categorize the biological functions of each subcluster into eight groups: hypoxia (clusters 0 and 14), cell adhesion (clusters 1 and 13), cell cycle (clusters 2, 3, 6, 7, and 11), ribosome or mitochondrial overexpression (cluster 4), neutrophil aggregation (clusters 5 and 15), serine metabolic process (clusters 8 and 10), pluripotency (clusters 9 and 12), mesenchyme development (cluster 16), and interferon signaling (cluster 17) (Fig. 2 *B* and *C*).

In general, cancer cells from macromet and PT displayed similar yet diverse transcriptional patterns, while tumor cells from micromet exhibited unique transcriptional activities and biological functions. Notably, three rare clusters (clusters 9, 12, and 16)

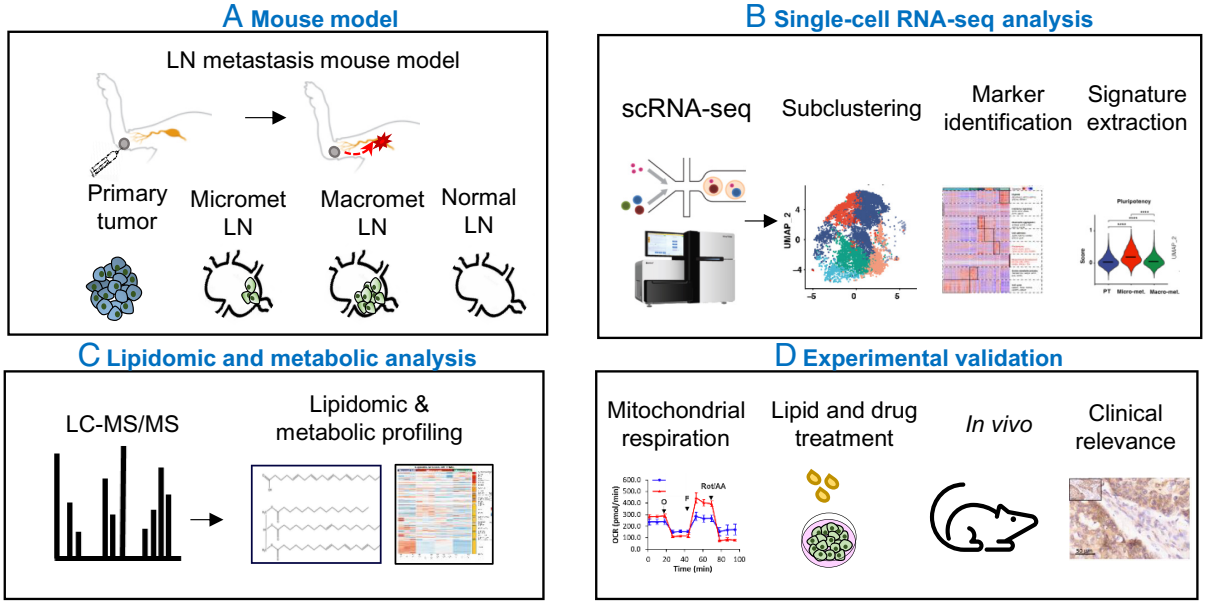

Fig. 1. Schematic overview of the study. (*A*) LN metastasis mouse model: Establishment of a LN metastasis mouse model to investigate tumor progression in primary tumors, micrometastatic (Micromet) LNs, macrometastatic (Macromet) LNs. (*B*) Single-cell RNA-seq analysis: Subclustering, marker identification, and signature extraction were performed to characterize tumor cell populations in LN metastases. (*C*) Lipidomic and metabolic analysis: Liquid chromatography was used to profile lipid composition and metabolic alterations in the LN metastatic microenvironment and tumor cells. (*D*) Experimental validation: Functional assays, including mitochondrial respiration measurements, lipid and drug treatments, in vivo metastasis models, and clinical relevance analysis were conducted to validate key findings.

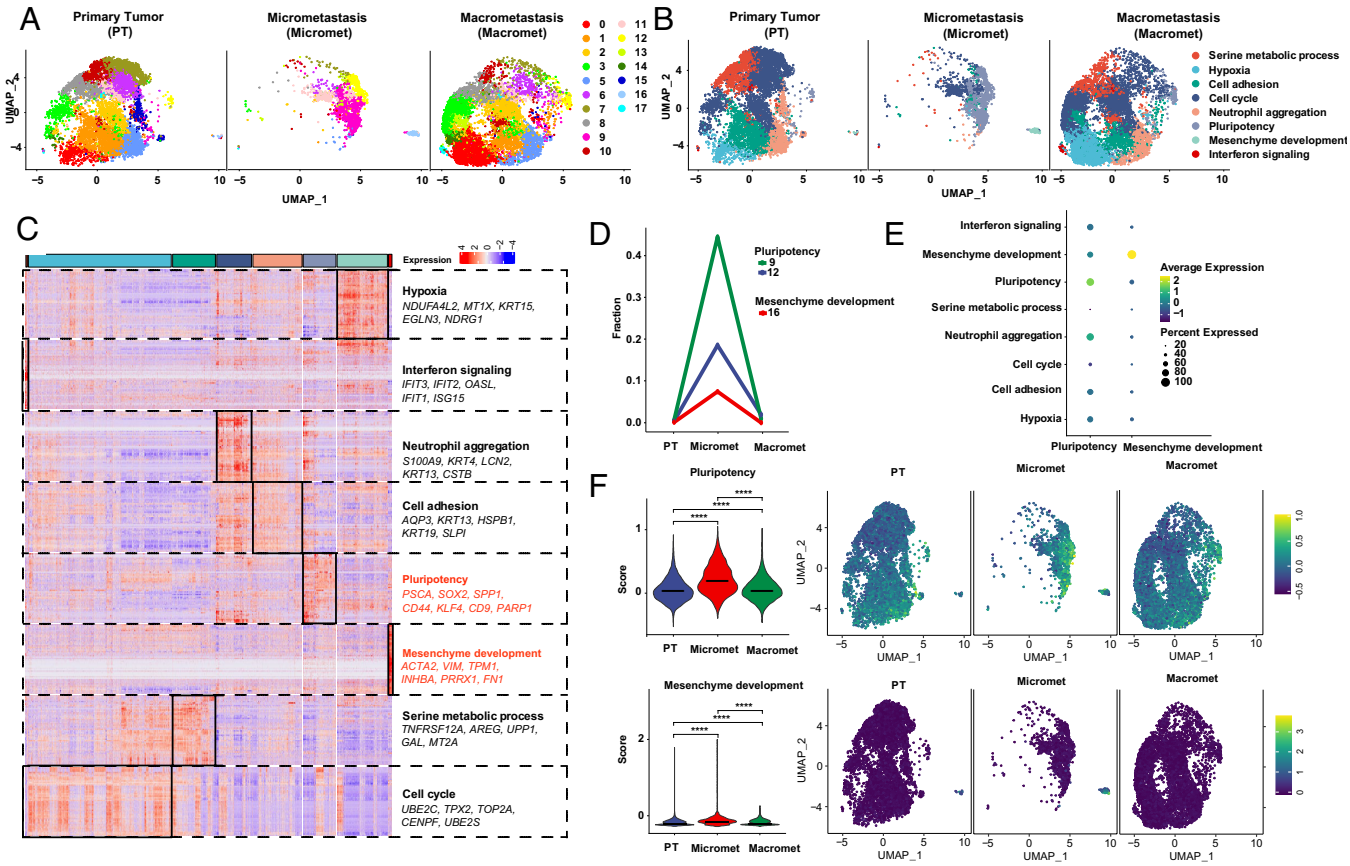

Fig. 2. Characterizing intratumor heterogeneity and molecular signatures of LN metastasis using single-cell transcriptomics. (*A*) Subclustering of tumor cells from primary tumor tissues (N = 7,334) and LNs with micromet (N = 2,037) or macromet (N = 9,206). (*B*) Categorization of the biological functions of each subcluster. (*C*) Diverse transcriptional patterns of 8 categories of tumor cells and identification of their signature markers. (*D*) Enrichment of tumor cell subsets associated with pluripotency (subclusters 9 and 12) and mesenchyme development (subcluster 16) in LNs with micromet. (*E*) Scaled expression score of pluripotency and mesenchyme development signatures across different categories of tumor cells. (*F*) Comparison of the pluripotency and mesenchyme development signature scores in tumor cells from PT and different stages of LN metastasis. Wilcoxon signed-rank test. **** $P < 0.0001$.

representing less than 3% of cells in primary tumors were significantly enriched up to 70% in micromet but were scarcely present in macromet (Fig. 2*D*). This observation suggests a pivotal role of these cell subsets in initiating LN metastasis. Clusters 9 and 12, associated with pluripotency, predominantly expressed stemness-regulating genes such as *SOX2*, *SPP1*, *PSCA*, *CD44*, *KLF4*, *CD9*, and *PARP1* (22) (*SI Appendix*, Fig. S2). Meanwhile, the mesenchyme-like cluster 16 displayed increased expression of mesenchymal development-related genes, including *ACTA2*, *VIM*, *TPM1*, and *FN1* (Fig. 2 *C*–*E*). A quantitative analysis of pluripotency and mesenchymal signatures across these tumor cells demonstrated significantly higher levels of these signatures in micromet sites compared to primary and macromet LNs (Fig. 2*F*). Collectively, single-cell analysis revealed distinct subpopulations, highlighting the heterogeneity and identifying potential MICs that support a hierarchical model of metastasis (23, 24).

Distinctly Enhanced Metastatic Behavior of Tumor Cells Isolated from Micrometastatic LNs. Given the predominant enrichment of potential MICs in micromet LNs, we isolated tumor cells from this context (LNM) and conducted comparative molecular and functional analyses against tumor cells derived from primary tumors (PT) (Fig. 3*A*). The upregulation of stemness regulatory genes was detected in LNM cells compared with PT (Fig. 3*B*). LNM cells also exhibited a superior capacity to form tumor spheroids with elevated SOX2 levels, indicating enhanced stem-like characteristics (Fig. 3 *C* and *D*). Although LNM cells showed comparable proliferation rates to PT cells (*SI Appendix*, Fig. S3*A*), they demonstrated increased mobility and invasive properties, as evidenced by Transwell assays and the expression of mesenchymal markers (*SI Appendix*, Fig. S3 *B* and *C*).

To compare the tumorigenic and metastatic potentials of LNM and PT cells, we reinoculated tumor cells into mice and monitored tumor growth and metastasis in LNs and lungs. Our findings revealed that LNM cells exhibited extensive spontaneous metastasis to both LNs and lungs compared to PT cells (Fig. 3 *E* and *F*), with no significant difference in primary tumor size (*SI Appendix*, Fig. S3*D*). Further investigation through tail vein injection of LNM cells into mice demonstrated prolonged circulatory persistence and a marked increase in lung colonization compared to PT cells (Fig. 3 *G* and *H*), ultimately leading to reduced survival (Fig. 3*I*). Together, these results underscore the critical role of MICs in promoting metastatic dissemination through lymphatic and hematogenous routes.

OXPHOS Dependency Characterizes MICs. Metabolic rewiring is essential for tumor cells to adapt to the metastatic cascade. scRNA-seq analysis of MIC clusters with non-MIC clusters revealed a pronounced shift toward OXPHOS and enhanced responses to oxidative stress, indicating a reliance on OXPHOS in LN metastatic cells (Fig. 4*A*). Whole-transcriptome analysis corroborated the upregulation of OXPHOS-related genes in LNM compared to PT cells (*SI Appendix*, Fig. S4 *A* and *B*). The enhanced reliance on OXPHOS in LNM, was evident through increased mRNA expression of mitochondrial biogenesis and electron transport chain components (PGC1α, MT-RNR,

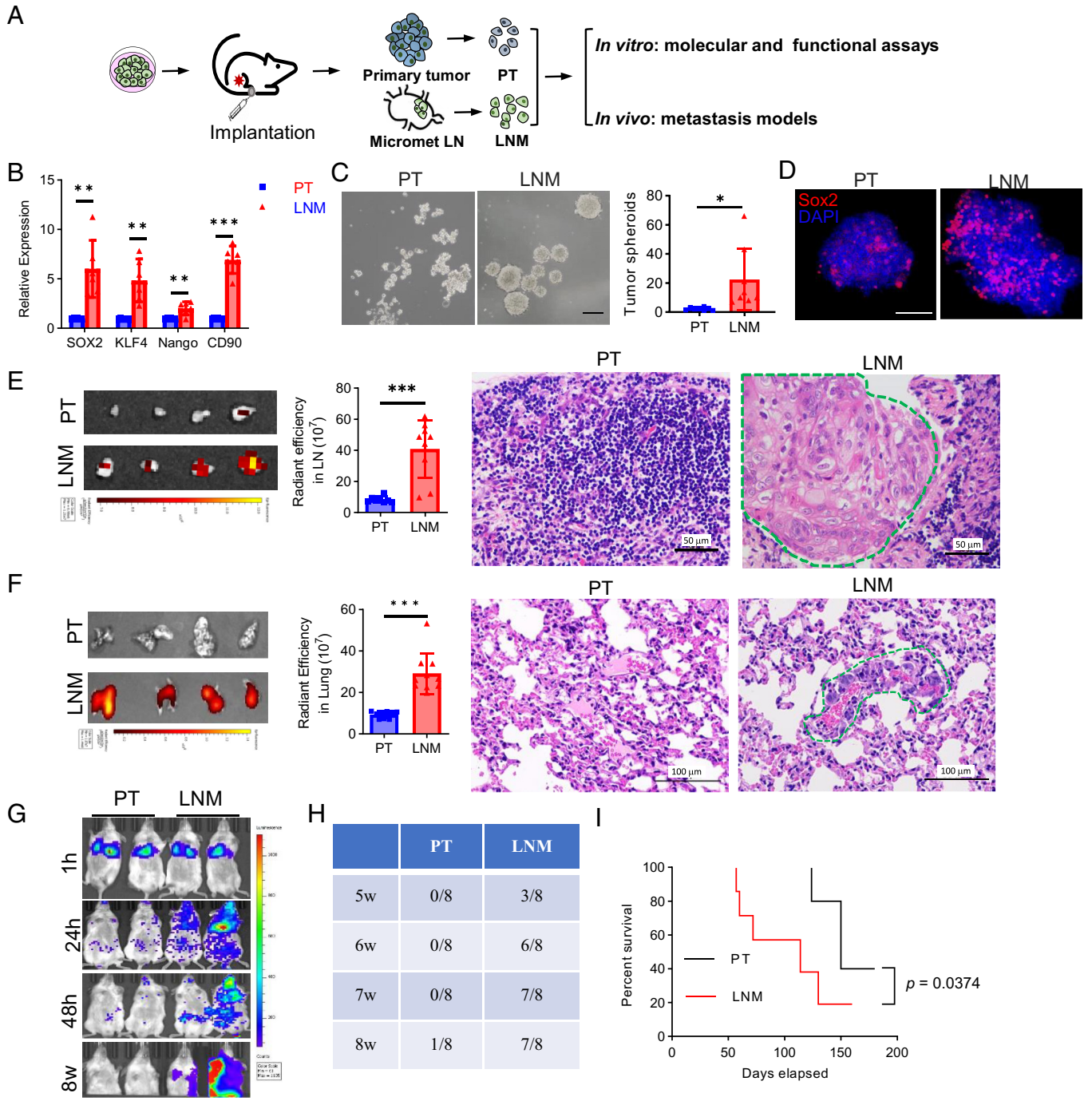

	PT	LNM
5w	0/8	3/8
6w	0/8	6/8
7w	0/8	7/8
8w	1/8	7/8

Fig. 3. Early disseminated tumor cells in LN possess a distinct metastasis-initiating potential. (*A*) Schematic of the experimental setup for isolation and characterization of tumor cells in micromet LN. (*B*) Quantitative PCR validation of pluripotency markers in PT and LNM cells. N = 6. (*C*) Representative images and quantitation of tumor spheroids of PT and LNM cells. (Scale bar, 100 μm.) (*D*) Confocal microscopy for SOX2 in tumor spheroids. (Scale bar, 50 μm.) (*E* and *F*) Representative fluorescence images, quantification of fluorescent signal, and histology of excised LNs (*E*) and lungs (*F*) from mice s.c. inoculated with PT or LNM cells. (*G* and *H*) Representative bioluminescence imaging (BLI) images (*G*) and incidence of lung metastasis (*H*) in mice at different times after i.v. injection of tumor cells. (*I*) Kaplan–Meier survival curve for mice inoculated with PT or LNM cells. N = 7 mice. Data are presented as the mean ± SD. *B*, *C*, *E*, *F*, unpaired two-tailed Student's *t* test; *I*, log-rank test. ns, not significant; *$P < 0.05$; **$P < 0.01$; *** $P < 0.001$; **** $P < 0.0001$.

COX5B, and COX7B) (Fig. 4*B*). Elevated mitochondrial mass and functionality were confirmed by enhanced Mito Tracker signal and elevated TMRE fluorescence (Fig. 4 *C* and *D*). Transmission electron microscopy revealed healthy mitochondria with well-defined cristae in LNM cells, contrasting with the compromised mitochondria in PT cells (Fig. 4*E*). Seahorse Mito Stress assay results showed that LNM cells have higher respiratory capacities indicative of robust mitochondrial oxidative metabolism (Fig. 4*F*). These results affirm OXPHOS as a critical metabolic pathway for MICs.

Metabolic Shift Toward FAO Fuels Metastatic Phenotypes in LN Disseminated Tumor Cells. Tumor cells adapt to lipid-rich environments, like LN or omentum, by leveraging lipid for energy production, especially in conditions where glucose availability is limited (25, 26). FAO, a primary pathway in lipid catabolism, efficiently generates energy through OXPHOS. Lipidomic profiling of LN tissues revealed a significant depletion of overall lipid content in metastatic LNs compared to healthy ones (Fig. 5*A* and *SI Appendix*, Fig. S5*A*). Among the dysregulated lipid species, triacylglycerols (TGs) and diacylglycerols (DGs)

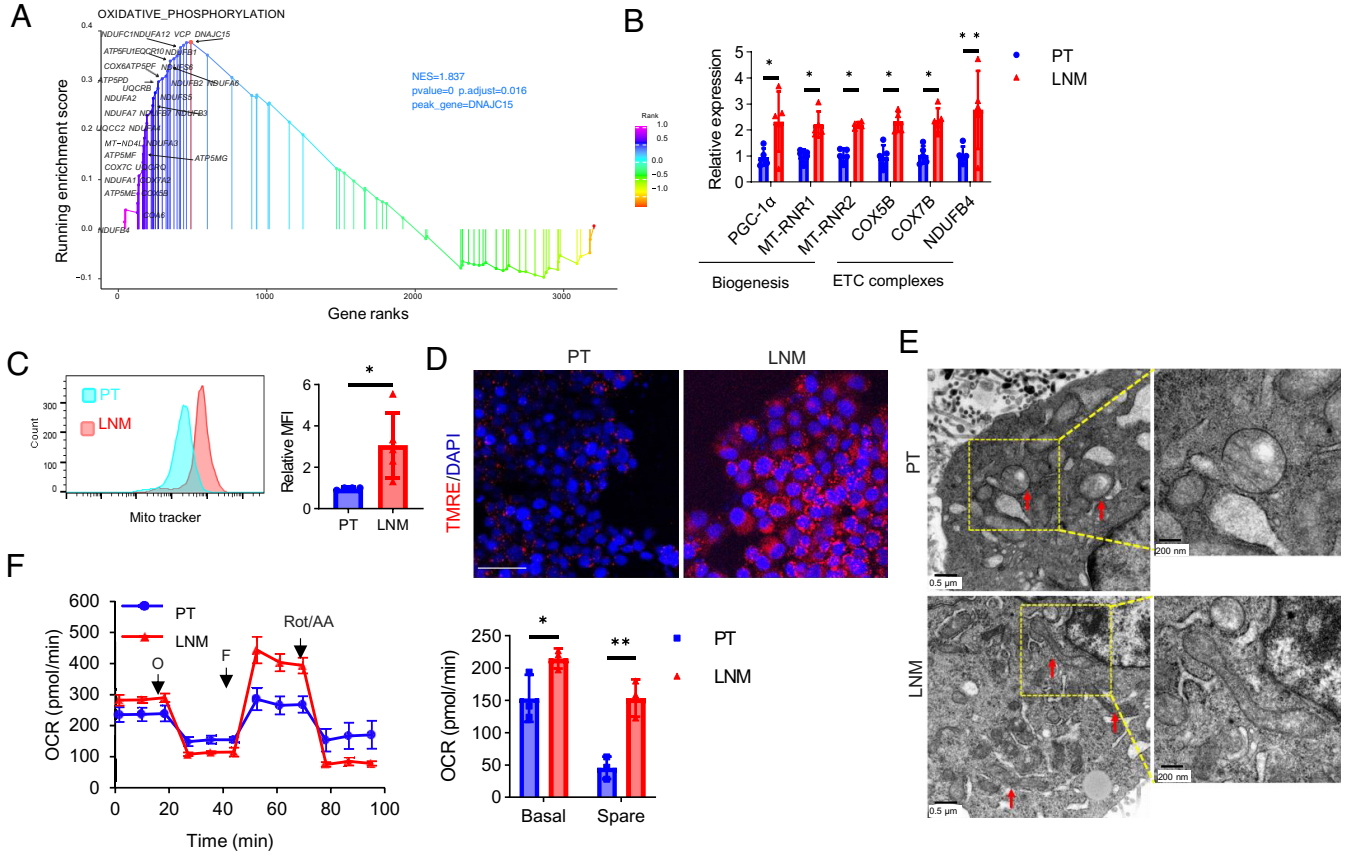

Fig. 4. Enhanced mitochondrial OXPHOS of metastatic tumor cells in early metastatic LNs. (*A*) GSEA plots illustrating upregulation of the OXPHOS pathway in MIC cluster. (*B*) Quantitative PCR validation of genes involved in mitochondrial biogenesis, ETC complexes in LNM normalized to PT. N = 5 biological replicates. (*C*) Representative FACS analysis and quantification of mitochondrial mass in PT and LNM stained with MitoTracker. N = 5 biological replicates. (*D*) Representative confocal images of tumor cells stained for mitochondria (TMRE, red) and DNA (DAPI). (Scale bar, 50 μm.) (*E*) Transmission electron microscopy of PT and LNM cells. Arrowheads indicate mitochondria. (Scale bars of *Left* panel, 0.2 μm *Right* panel 100 nm.) (*F*) OCR measurements and histogram of spare respiratory rates in PT and LNM cells. O, oligomycin; F, FCCP; Rot/AA, rotenone with antimycin. N = 3 biological replicates. Data are presented as the mean ± SD, unpaired two-tailed Student's *t* test. ns, not significant; *$P < 0.05$; **$P < 0.01$.

showed the most pronounced reductions (Fig. 5 *A* and *B* and *SI Appendix,* Fig. S5 *B–D*), suggesting lipid mobilization during metastasis. Metabolomic analysis revealed increased acyl-carnitines in LNM cells, reflecting elevated FAO activity (Fig. 5*C*). Transcriptomic data further demonstrated upregulated lipid catabolism and downregulated lipogenesis in MICs (Fig. 5*D* and *SI Appendix*, Fig. S5*E*). RT-PCR confirmed the upregulation of lipid catabolism genes, including CD36, ATGL, and CPT1, alongside downregulation of fatty acid synthase (FASN) in LNM (Fig. 5*E*). Enhanced fatty acid uptake and storage were further validated by increased BODIPY FL- C12 and BODIPY 493/503 staining in LNM (Fig. 5 *F* and *G*). Collectively, these findings suggest that MICs adapt to the lipid-rich LN microenvironment by enhancing lipid uptake and FAO-driven OXPHOS to meet their energy demands.

To assess the impact of fatty acids (FAs) on tumor progression, we analyzed the changes in specific FAs in LNs during metastasis. The predominant saturated and unsaturated FAs—palmitic (PA) and linoleic acid (LA)—were reduced in metastatic LNs compared to healthy LNs (Fig. 6 *A* and *B*). In vitro, supplementation with PA and LA enhanced mitochondrial respiration (Fig. 6*C*), spheroid formation with increased SOX2 expression (Fig. 6 *D* and *E*), and cell mobility (Fig. 6*F*), indicating their role in promoting metastatic properties. In vivo, tumor cells pretreated with PA and LA exhibited increased LN and lung metastasis (Fig. 6 *G* and *H*), and tumor-bearing mice on a high-fat diet exhibited higher metastatic burden compared to those on a control diet (Fig. 6*I*). Pharmacological inhibition of FAO using etomoxir selectively reduced LN metastasis without affecting primary tumor growth or lung metastasis (Fig. 6*J* and *SI Appendix,* Fig. S6 *A* and *B*). These findings highlight FAO as a key metabolic pathway facilitating lymphatic metastasis in cancer.

NRF2 Regulates Ferroptosis Resistance Through GSH System in MICs. Metabolic reprogramming toward OXPHOS inherently produces mitochondrial superoxide (mtROS), a major source of intracellular ROS, posing significant oxidative stress to tumor cells and requiring robust antioxidant defenses. Bioinformatic analyses and WB revealed elevated NRF2 and its downstream target SLC7A11 in MICs, key regulators of GSH synthesis and oxidative defense (Fig. 7 *A–C* and *SI Appendix*, Figs. S7 *A* and *B* and S12) (18, 27, 28). Tumor cells cultured in FA-supplemented medium exhibited increased NRF2 and SLC7A11expression (*SI Appendix*, Figs. S7*C* and S13), highlighting their role in adapting tumor cells to the LN microenvironment.

Though there was no significant difference at baseline, mtROS levels were markedly lower in LNM cells than in PT cells upon oxidative induction with the GSH-depleting agent IKE (*SI Appendix,* Fig. S8 *A* and *B*). LNM also displayed lower baseline lipid peroxidation and only modest elevation upon oxidative induction, further confirming their superior redox balance and enhanced antioxidant capacity (Fig. 7*D*). Moreover, LNM displayed higher GSH level and GSH/GSSG ratio relative to PT cells, reflecting enhanced intracellular GSH capacity in MICs

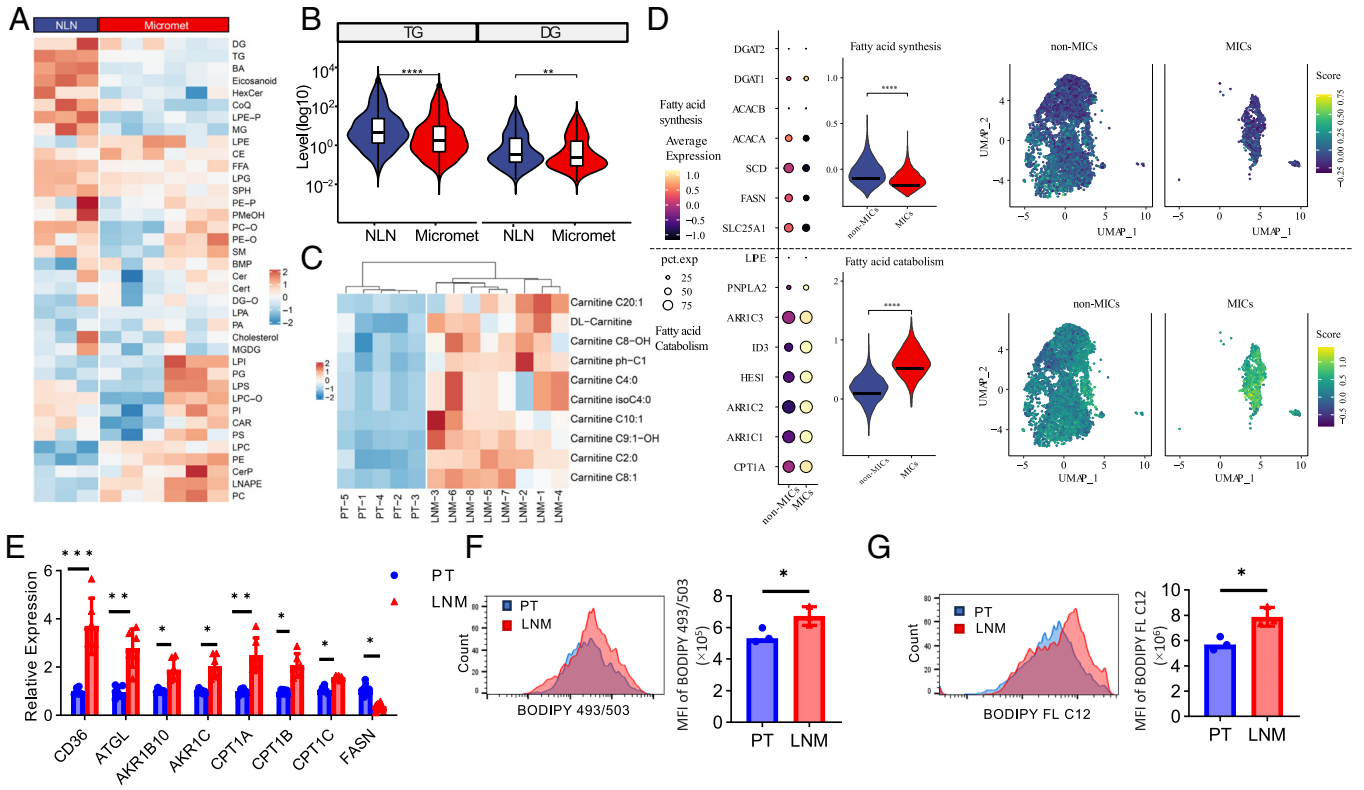

Fig. 5. Integrative Transcriptomic and Lipidome Analysis Identifies Lipid Metabolism Signature Associated with LN Metastasis. (*A*) Heatmap showing lipid species abundance identified in normal (NLN) and micromet LN. N = 3 (NLN); 6 (Micromet LNs). (*B*) Levels of triacylglycerols (TG) and diacylglycerols (DG) in normal LNs and micromet LNs. (*C*) Heatmap showing unsupervised clustering of carnitine compounds abundance in PT and LNM cells. N = 5 (PT); 8 (LNM) biological replicates. (*D*) Comparison of de novo lipogenesis and lipid catabolism signature scores in MICs and non-MICs. (*E*) Quantitative PCR validation of genes involved in fatty acid utilization and synthesis in LNM normalized to PT. N = 5 biological replicates. (*F* and *G*) Quantification of neutral lipid content (*F*) and lipid uptake (*G*) in PT and LNM cells using BODIPY staining. Data are presented as the mean ± SD. *B–D*, Wilcoxon signed-rank test; *E–G*, Unpaired two-tailed Student's *t* test. ns, not significant; **P* < 0.05; ***P* < 0.01; *** *P* < 0.001; **** *P* < 0.0001.

(Fig. 7*E*). NAC or Ferr-1 treatment reduced ROS levels and rescued cell viability, confirming ferroptosis as the primary mode of cell death (*SI Appendix*, Fig. S8 *A* and *B*) (29) (30).

NRF2 silencing in LNM reduced GSH synthesis and impaired stress resistance, which could be rescued by NAC or Ferr-1 (Fig. 7*F* and *SI Appendix*, Figs. S9*A* and S14). Conversely, NRF2 overexpression enhanced ferroptosis resistance by maintaining GSH levels (*SI Appendix*, Figs. S9 *B–F* and S15). NRF2 inhibitor ML385 sensitized LNM cells to IKE-induced ferroptosis (*SI Appendix*, Fig S9*G*). Critically, the role of NRF2 in maintaining redox balance was dependent on SLC7A11, as NRF2-related antioxidant effects were reversed by SLC7A11 manipulation (Fig. 7 *F* and *G* and *SI Appendix*, Fig. S9 *A–I*).

LNM also showed enhanced cisplatin resistance compared to PT, which could be reversed by NRF2 or SLC7A11 inhibition (Fig. 7 *H* and *I*). Similarly, NRF2-OE cells displayed heightened cisplatin resistance, an effect mitigated by SLC7A11 silencing (*SI Appendix*, Fig S9*H*). In vivo, NRF2-OE tumor cells exhibited enhanced LN metastatic potential (Fig. 7*J* and *SI Appendix*, Fig. S9*I*), while pharmaceutical inhibition of NRF2 or SLC7A11 significantly reduced LN metastasis in mice bearing LNM tumors (Fig. 7 *K* and *L*). Notably, combining NRF2 or SLC7A11 inhibitors with cisplatin more effectively suppressed tumor growth and LN metastasis than either treatment alone (Fig. 7 *K* and *L*).

These findings highlight the NRF2-SLC7A11 axis as a critical mechanism in MICs, enhancing GSH-mediated redox balance and stress resistance during LN metastasis. Targeting this axis provides a promising therapeutic approach to overcome cisplatin resistance in MICs.

Clinical Significance of NRF2 Signaling in LN Metastasis and Chemoresistance in ESCC. To evaluate the clinical relevance of our findings, scRNA-seq data from ESCC patients revealed significant upregulation of pluripotency, OXPHOS dependency, and NRF2-mediated stress response pathways in tumor cells within LN metastases compared to normal epithelial cells (Fig. 8*A* and *SI Appendix*, Fig. S10) (31). IHC analysis of tissue microarrays confirmed elevated NRF2 and SLC7A11 protein levels in primary tumors, with minimal expression in matched normal tissues (Fig. 8*B*). NRF2 and SLC7A11 expression were positively correlated (Fig. 8*C* and *SI Appendix*, Fig. S11*A*), and NRF2 expression was significantly higher in tumors with LN metastases compared to those without (Fig. 8*D* and *SI Appendix*, Fig. S11*B*).

In a chemotherapy-treated ESCC cohort, high NRF2 expression was significantly associated with poor response to chemotherapy (Fig. 8*E*). Kaplan–Meier analysis demonstrated that high NRF2 expression was associated with poor overall survival (Fig. 8*F* and *SI Appendix*, Fig. S11*C*). Multivariate analysis identified NRF2 as an independent prognostic factor for reduced survival (HR: 2.39, 95% CI: 1.08 to 5.33, *P* = 0.032) (*SI Appendix*, Tables S1 and S2). These findings highlight NRF2's role in promoting LN metastasis and chemoresistance, suggesting its potential as a prognostic biomarker and therapeutic target.

Discussion

Understanding the early molecular and metabolic adaptations enabling tumor cells to thrive in the LN microenvironment remains limited. This study identifies rare MICs with stem-like

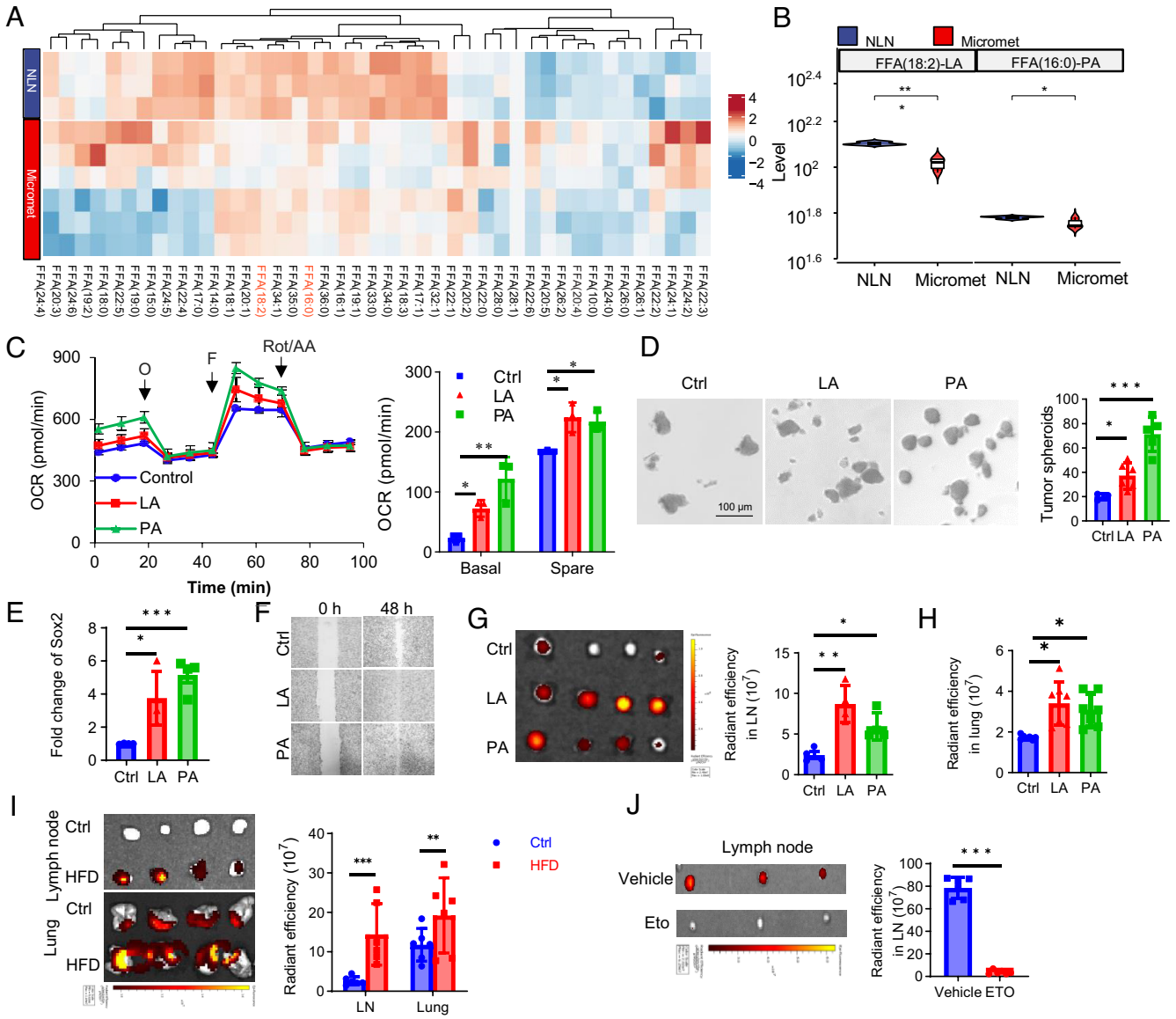

Fig. 6. FAs fuel OXPHOS to facilitate tumor LN metastasis. (*A*) Heatmap of 43 lipid compounds of free FAs in normal and metastatic LNs. (*B*) Comparison of LA and PA levels in normal and metastatic LNs. (*C*) OCR measurements and histogram of respiration rates in KYSE-180 cells treated with or without FAs (50 μM PA or LA for 48 h). N = 3 biological replicates. (*D*) Images (*Left*) and quantification (*Right*) of tumor spheroids formed by KYSE-180 cells treated with FAs. (Scale bar, 100 μm.) N = 4 biological replicates. (*E*) Relative SOX2 mRNA levels in FAs-treated KYSE-180 cells. N = 4 biological replicates. (*F*) Evaluation of FA effects on tumor cell mobility. (*G* and *H*) Images and quantification of fluorescent signals in LNs (*G*) and lungs (*H*) of GFP-luciferase-labeled KYSE-180 s.c. implanted mice. Tumor cells were cultured with 50 μM PA or LA for 96 h prior to implantation. (*I*) Images and quantification of fluorescent signals in LNs and lungs of mice s.c. inoculated with GFP-luciferase-labeled KYSE-180 cells and fed basal or high-fat diets. N = 6 mice. (*J*) Images and quantification of fluorescent signals in LNs of GFP-luciferase-labeled KYSE-180 tumor-bearing mice treated with or without etomoxir. N = 5 mice. Data are presented as the mean ± SD. *B*, Wilcoxon signed-rank test; *C–E*, *G* and *H* one-way ANOVA, *I* and *J* unpaired student *t* test. ns, not significant; **P* < 0.05; ***P* < 0.01; ****P* < 0.001.

properties that exhibit a metabolic dependence on FAO-fueled OXPHOS, driving LN metastasis. We extend previous findings by demonstrating that FAO not only sustains energy production under nutrient-limited conditions but also actively enhances the metastatic phenotype of MICs, highlighting its role as a critical driver of metastatic competence (26, 32).

Our findings underscore the importance of FAO as a central metabolic pathway fueling OXPHOS during LN metastasis. Lipidomic, metabolomic, and transcriptomic analyses revealed significant lipid mobilization in metastatic LNs, characterized by a pronounced depletion of TG and DG. MICs exhibited upregulated lipid catabolism and reduced lipogenesis, with increased expression of FAO-related genes, and decreased FASN. Enhanced fatty acid uptake and storage in MICs further supported their metabolic reliance on FAO for energy demands during LN colonization. While FAO appears to dominate LN metabolic adaptations, other carbon sources such as glutamine and glucose may contribute to OXPHOS and warrant further investigation (26, 33, 34).

Experimental evidence validated the functional significance of FAO in metastatic progression. FA supplementation increased mitochondrial respiration, spheroid formation, and cell mobility. In vivo, FA treatment promoted LN and lung metastasis, while pharmacological inhibition of FAO using etomoxir selectively reduced LN metastasis without affecting primary tumor growth or lung metastasis. These results establish FAO as a critical metabolic adaptation supporting MIC fitness in the LN microenvironment.

MICs demonstrated superior oxidative stress resistance, a critical survival mechanism during metastasis (8, 15, 35). MICs rely on NRF2-SLC7A11 signaling to enhance GSH synthesis, maintaining redox balance and mitigating oxidative stress. This pathway

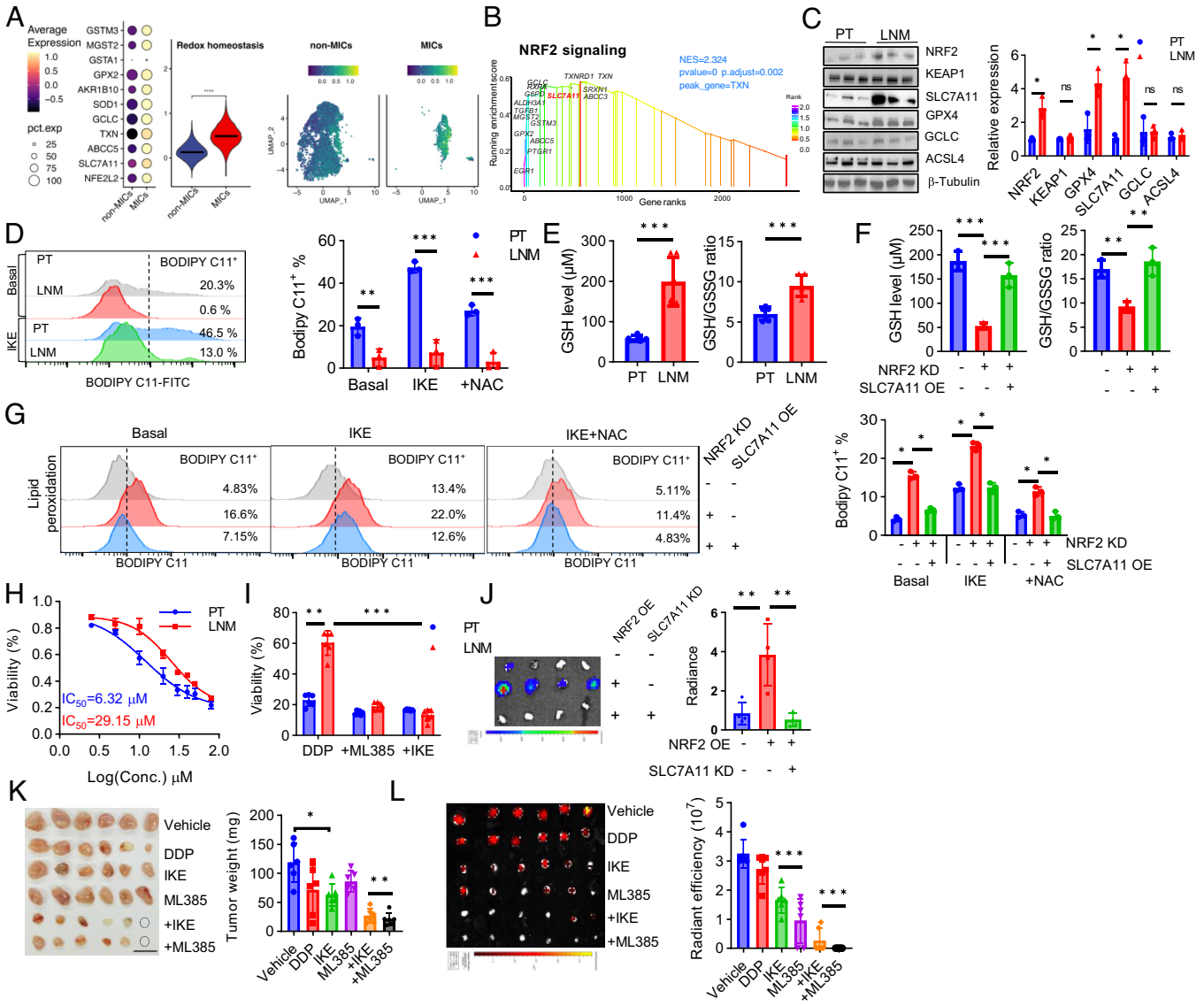

Fig. 7. NRF2-SLC7A11 signaling protects ESCC cells from ferroptosis and enhances LN metastasis. (*A*) Scaled expression score of redox homeostasis signature of MICs and non-MICs. (*B*) GSEA plot illustrating upregulation of NRF2 signaling in MICs with GSH synthesis genes highlighted in red. (*C*) WB of NRF2 signaling proteins in PT and LNM cells. N = 3 biological replicates. (*D*) Lipid peroxidation levels in PT and LNM cells treated with or without IKE (40 μM). N = 3 biological replicates. (*E* and *F*) GSH levels and GSH/GSSG ratios in PT and LNM cells (*E*), LNM cells with or without NRF2-SLC7A11 manipulation (*F*). N = 6 biological replicates. (*G*) Lipid peroxidation levels in NRF2-silenced LNM cells with or without SLC7A11 overexpression treated with IKE. N = 3 biological replicates. (*H*) Viability curves and IC_{50} values of PT and LNM cells treated with cisplatin (DDP) for 24 h. N = 3 biological replicates. (*I*) Viability of PT and LNM cells treated with DDP (10 μM) in combination with ML385 (2 μM) or IKE (20 μM) for 48 h. N = 6 biological replicates. (*J*) BLI image and quantification for LN metastasis in mice bearing luciferase-labeled KYSE-30 cells. N = 4 mice. (*K* and *L*) Tumor weight (*K*) and LN metastasis (*L*) in mice bearing GFP-luciferase-labeled LNM cells. Mice were treated with DDP (30 mg/kg) with or without IKE (40 mg/kg) or ML385 (30 mg/kg). N = 6 mice. Data are presented as the mean ± SD. *A*, Wilcoxon signed-rank test; *B*, permutation test; *C*, *E*, *H*, unpaired Student's *t* test; *D* Two-way ANOVA; *F*, *J*–*L*, one-way ANOVA: * $P < 0.05$; ** $P < 0.01$; *** $P < 0.001$; **** $P < 0.0001$.

supports MIC survival under oxidative conditions and contributes to ferroptosis resistance. Notably, inhibition of NRF2 or SLC7A11 impaired MIC stress resistance, reduced LN metastasis, and sensitized tumor cells to cisplatin in vitro and in vivo. These findings suggest that the NRF2-SLC7A11 axis is a key mediator of MIC resilience and survival during metastasis.

Clinically, elevated NRF2-SLC7A11 expression was positively associated with LN metastasis, chemoresistance, and poor survival in ESCC patients. Targeting NRF2-SLC7A11 in combination with standard chemotherapy improved treatment efficacy, reducing tumor growth and LN metastasis. These findings suggest that combining ferroptosis inducers with chemotherapeutic agents offers a promising strategy to treat metastatic cancer (32, 36).

In conclusion, this study highlights FAO-fueled OXPHOS and NRF2-mediated oxidative stress resistance as pivotal mechanisms underpinning MIC metabolic fitness and resilience, driving LN metastasis. Targeting these pathways holds promise for improving therapeutic outcomes in metastatic cancers.

Methods

Ethical Approval and Informed Consent. This study was conducted in accordance with ethical standards and approved protocols. Informed consent was obtained from all human participants prior to sample collection. The study protocol for human subjects was reviewed and approved by the Research Ethics Committee of The First Affiliated Hospital of Zhengzhou University and the Medical Ethics Committee of Sun Yat-sen University Cancer Center.

Animal experiments were conducted following the guidelines set by the Committee on the Use of Live Animals in Teaching and Research at the University of Hong Kong. All animal procedures were approved under the institutional protocol.

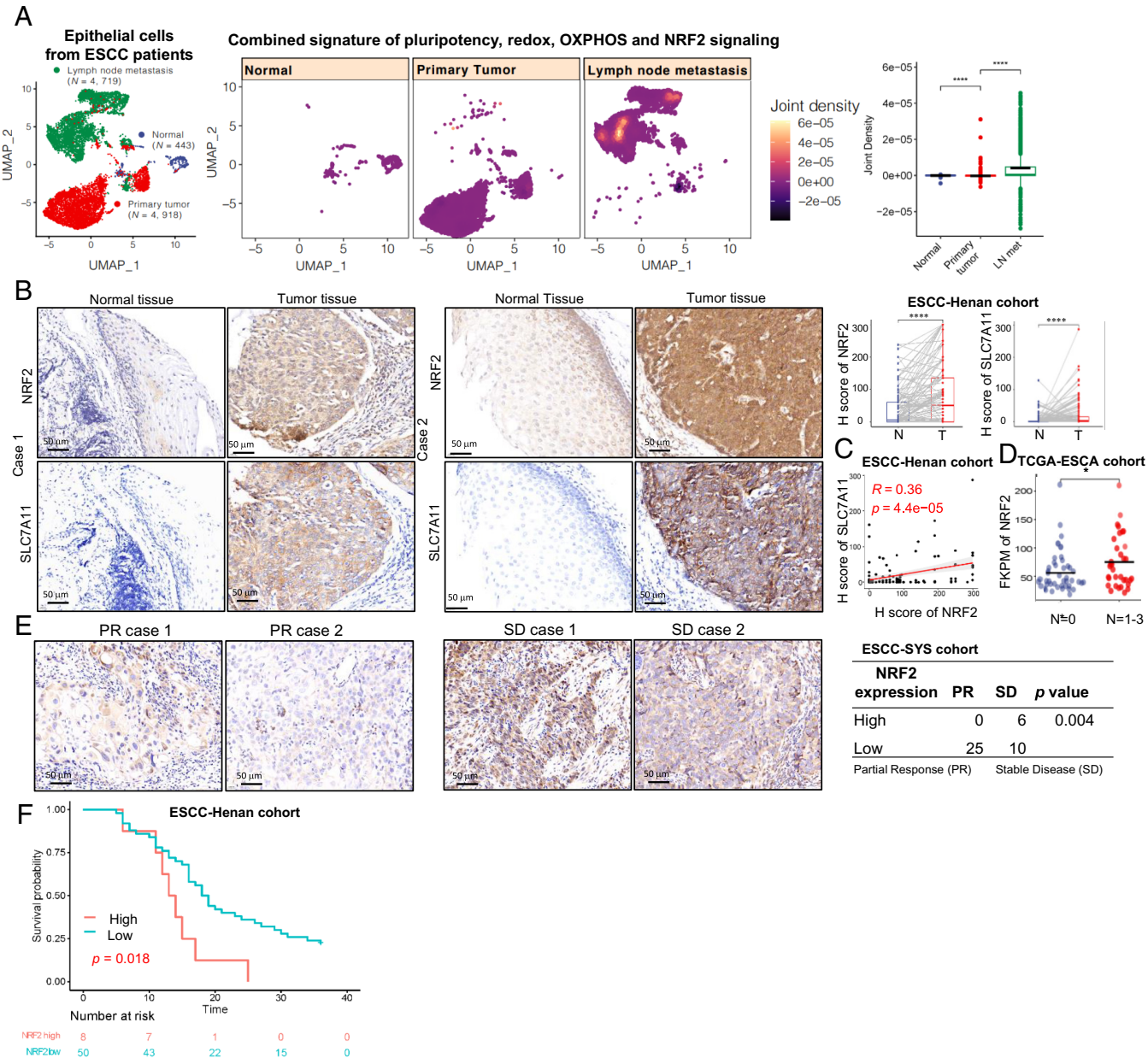

Fig. 8. Clinical Significance of NRF2 Signaling in LN Metastasis and Chemoresistance in ESCC. (*A*) UMAP and joint density maps showing pluripotency, redox balance, OXPHOS and NRF2 signature in normal epithelial cells, primary tumor cells and LN metastatic cells from scRNA-seq data from ESCC patients. (*B*) Representative IHC images and quantification of NRF2 and SLC7A11 protein levels in normal (N) and tumor (T) tissues in ESCC-Henan cohort. N = 123 patients. (*C*) Pearson correlation between NRF2 and SLC7A11 protein levels in the ESCC-Henan cohort. N = 123 patients. (*D*) Representative IHC images and statistical analysis of NRF2 expression in relation to chemotherapy response. N = 41 patients from ESCC-SYS cohort. (*E*) Transcript levels of NRF2 in TCGA-ESCA samples stratified by LN metastasis status. N0: 44; N1-3: 34 patients. (*F*) Kaplan–Meier survival analysis of overall survival stratified by NRF2 expression. N = 58 patients from ESCC-Henan cohort with survival data. *A*, Wilcoxon signed-rank test; *B*, paired student's *t* test; *C*, Pearson correlation analysis; *D*, chi-square analysis; *E*, unpaired student's *t* test; *F*, log-rank test. **P* < 0.05, **** *P* < 0.0001.

Other Materials and Methods. Additional details of experimental methods, reagents, and procedures are provided in *SI Appendix, Supporting Methods*.

Data, Materials, and Software Availability. The raw sequencing data and processed data of scRNA-seq and bulk RNAseq of this study were submitted and will be available in the Gene Expression Omnibus (GEO) database https://www.ncbi.nlm.nih.gov/geo/ under Accession code GSE220108 (37). All other data is included in the manuscript and/or *SI Appendix*.

ACKNOWLEDGMENTS. Shenzhen Medical Research Funds A2303060 (S.-S.L.), Shenzhen Science and Technology Program JCYJ20220530142409021 (S.-S.L.), JCYJ20220818103012025 (S.-S.L. and S.M.), ZDSYS20210623091811035 (X.-Y.G. and A.W.-M.L.), KQTD20180411185028798 (X.-Y.G.), RCBS20221008093232045 (H.W.), National Natural Science Foundation of China 82103643 (S.-S.L.), 82072731 (W.C.), 82202857 (H.W.), High Level-Hospital Program, Health Commission of Guangdong Province HKUSZH201901002 (A.W.-M.L.), Sanming Project of Medicine in Shenzhen SZSM202211017 (A.W.-M.L.), X.-Y.G. is the Sophie YM Chan Professor in Cancer Research.

Author affiliations: [a]Shenzhen Key Laboratory for Cancer Metastasis and Personalized Therapy, Department of Clinical Oncology, The University of Hong Kong-Shenzhen Hospital, Shenzhen 518000, China; [b]Advanced Energy Science and Technology Guangdong Laboratory, Huizhou 516007, China; [c]Department of Clinical Oncology, Li Ka Shing Faculty of Medicine, The University of Hong Kong, Hong Kong 999077, China; [d]Department of Medical Oncology, State Key Laboratory of Oncology in South China, Guangdong Provincial Clinical Research Center for Cancer, Sun Yat-sen University Cancer Center, Guangzhou 510060, China; [e]School of Biomedical Sciences, Li Ka Shing Faculty of Medicine, The University of Hong Kong, Hong Kong 999077, China; [f]Guangdong Provincial Key Laboratory of Regional Immunity and Diseases, Department of Pharmacology and International Cancer Center, Shenzhen University Health Science Center, Shenzhen 518055, China; and [g]State Key Laboratory of Quantitative Engineering Biology, Shenzhen Institute of Synthetic Biology, Shenzhen Institutes of Advanced Technology, Chinese Academy of Sciences, Shenzhen 518055, China

1. H. Wang, F. Deng, Q. Liu, Y. Ma, Prognostic significance of lymph node metastasis in esophageal squamous cell carcinoma. *Pathol. Res. Pract.* **213**, 842–847 (2017).
2. A. W. Lambert, D. R. Pattabiraman, R. A. Weinberg, Emerging biological principles of metastasis. *Cell* **168**, 670–691 (2017).
3. K. Ganesh, J. Massague, Targeting metastatic cancer. *Nat. Med.* **27**, 34–44 (2021).
4. P. Mehlen, A. Puisieux, Metastasis: A question of life or death. *Nat. Rev. Cancer* **6**, 449–458 (2006).
5. M. Diehn, R. Majeti, Metastatic cancer stem cells: An opportunity for improving cancer treatment? *Cell Stem Cell* **6**, 502–503 (2010).
6. J. Massague, A. C. Obenauf, Metastatic colonization by circulating tumour cells. *Nature* **529**, 298–306 (2016).
7. D. Hanahan, Hallmarks of cancer: New dimensions. *Cancer Discov.* **12**, 31–46 (2022).
8. E. Piskounova *et al.*, Oxidative stress inhibits distant metastasis by human melanoma cells. *Nature* **527**, 186–191 (2015).
9. B. Faubert, A. Solmonson, R. J. DeBerardinis, Metabolic reprogramming and cancer progression. *Science* **368**, eaaw5473 (2020).
10. J. Hu *et al.*, Heterogeneity of tumor-induced gene expression changes in the human metabolic network. *Nat. Biotechnol.* **31**, 522–529 (2013).
11. K. Ohshima, E. Morii, Metabolic reprogramming of cancer cells during tumor progression and metastasis. *Metabolites* **11**, 28 (2021).
12. G. Pascual *et al.*, Targeting metastasis-initiating cells through the fatty acid receptor CD36. *Nature* **541**, 41–45 (2017).
13. C. M. Young *et al.*, Metabolic dependencies of metastasis-initiating cells in female breast cancer. *Nat. Commun.* **14**, 7076 (2023).
14. R. T. Davis *et al.*, Transcriptional diversity and bioenergetic shift in human breast cancer metastasis revealed by single-cell RNA sequencing. *Nat. Cell Biol.* **22**, 310–320 (2020).
15. A. Tasdogan, J. M. Ubellacker, S. J. Morrison, Redox regulation in cancer cells during metastasis. *Cancer Discov.* **11**, 2682–2692 (2021).
16. M. Peiris-Pages, U. E. Martinez-Outschoorn, F. Sotgia, M. P. Lisanti, Metastasis and oxidative stress: Are antioxidants a metabolic driver of progression? *Cell Metab.* **22**, 956–958 (2015).
17. A. Tasdogan *et al.*, Metabolic heterogeneity confers differences in melanoma metastatic potential. *Nature* **577**, 115–120 (2020).
18. M. Rojo de la Vega, E. Chapman, D. D. Zhang, NRF2 and the hallmarks of cancer. *Cancer Cell* **34**, 21–43 (2018).
19. G. M. DeNicola *et al.*, Oncogene-induced Nrf2 transcription promotes ROS detoxification and tumorigenesis. *Nature* **475**, 106–109 (2011).
20. D. B. Fox *et al.*, NRF2 activation promotes the recurrence of dormant tumour cells through regulation of redox and nucleotide metabolism. *Nat. Metab.* **2**, 318–334 (2020).
21. Y. Cui *et al.*, Whole-genome sequencing of 508 patients identifies key molecular features associated with poor prognosis in esophageal squamous cell carcinoma. *Cell Res.* **30**, 902–913 (2020).
22. L. Zeng, Y. Zhu, C. S. Moreno, Y. Wan, New insights into KLFs and SOXs in cancer pathogenesis, stemness, and therapy. *Semin Cancer Biol.* **90**, 29–44 (2023).
23. H. Hosseini *et al.*, Early dissemination seeds metastasis in breast cancer. *Nature* **540**, 552–558 (2016).
24. D. A. Lawson *et al.*, Single-cell analysis reveals a stem-cell program in human metastatic breast cancer cells. *Nature* **526**, 131–135 (2015).
25. T. V. Petrova, G. Y. Koh, Biological functions of lymphatic vessels. *Science* **369**, eaax4063 (2020).
26. C. K. Lee *et al.*, Tumor metastasis to lymph nodes requires YAP-dependent metabolic adaptation. *Science* **363**, 644–649 (2019).
27. I. S. Harris *et al.*, Glutathione and thioredoxin antioxidant pathways synergize to drive cancer initiation and progression. *Cancer Cell* **27**, 211–222 (2015).
28. J. K. M. Lim *et al.*, Cystine/glutamate antiporter xCT (SLC7A11) facilitates oncogenic RAS transformation by preserving intracellular redox balance. *Proc. Natl. Acad. Sci. U.S.A.* **116**, 9433–9442 (2019).
29. N. Takahashi *et al.*, 3D culture models with CRISPR screens reveal hyperactive NRF2 as a prerequisite for spheroid formation via regulation of proliferation and ferroptosis. *Mol. Cell* **80**, 828–844.e826 (2020).
30. L. Jiang *et al.*, Ferroptosis as a p53-mediated activity during tumour suppression. *Nature* **520**, 57–62 (2015).
31. Y. Jia *et al.*, Single-cell transcriptomic analysis of primary and metastatic tumor ecosystems in esophageal squamous cell carcinoma. *Adv. Sci. (Weinh)* **10**, e2204565 (2023).
32. Y. Wang *et al.*, ACSL4 and polyunsaturated lipids support metastatic extravasation and colonization. *Cell* **188**, 412–429.e427 (2025).
33. I. Elia *et al.*, Proline metabolism supports metastasis formation and could be inhibited to selectively target metastasizing cancer cells. *Nat. Commun.* **8**, 15267 (2017).
34. L. Yang *et al.*, Metabolic shifts toward glutamine regulate tumor growth, invasion and bioenergetics in ovarian cancer. *Mol. Syst. Biol.* **10**, 728 (2014).
35. C. Glorieux, S. Liu, D. Trachootham, P. Huang, Targeting ROS in cancer: Rationale and strategies. *Nat. Rev. Drug Discov.* **23**, 583–606 (2024).
36. J. M. Ubellacker *et al.*, Lymph protects metastasizing melanoma cells from ferroptosis. *Nature* **585**, 113–118 (2020).
37. S. Li, B. Zhang, X. Guan, FAO-fueled OXPHOS and NRF2-mediated stress resilience in MICs drive lymph node metastasis. NCBI Gene Expression Omnibus. https://www.ncbi.nlm.nih.gov/geo/query/acc.cgi?acc=GSE220108. Deposited 5 December 2022.